Pseudospectral calculation of helium wave functions, expectation values, and oscillator strength

Paul E. Grabowski and David F. Chernoff

Phys. Rev. A **84**, 042505 — Published 11 October 2011

DOI: 10.1103/PhysRevA.84.042505

Pseudospectral Calculation of Helium Wave Functions, Expectation Values, and Oscillator Strength

Paul E. Grabowski*

Department of Physics, Cornell University, Ithaca, NY 14853, USA†

David F. Chernoff‡

Department of Astronomy, Cornell University, Ithaca, NY 14853, USA

(Dated: August 30, 2011)

Abstract

We show the pseudospectral method is a powerful tool for finding precise solutions of Schrödinger's equation for two-electron atoms with general angular momentum. Realizing the method's full promise for atomic calculations requires special handling of singularities due to two-particle Coulomb interactions. We give a prescription for choosing coordinates and subdomains whose efficacy we illustrate by solving several challenging problems. One test centers around the determination of the nonrelativistic electric dipole oscillator strength for the helium $1^1\mathrm{S} \rightarrow 2^1\mathrm{P}$ transition. The result achieved, 0.27616499(27), is comparable to the best in the literature. The formally equivalent length, velocity, and acceleration expressions for the oscillator strength all yield roughly the same accuracy. We also calculate a diverse set of helium ground state expectation values, reaching near state-of-the-art accuracy without the necessity of implementing any special-purpose numerics. These successes imply that general matrix elements are directly and reliably calculable with pseudospectral methods. A striking result is that all the relevant quantities tested in this paper – energy eigenvalues, S-state expectation values and a bound-bound dipole transition between the lowest energy S and P states – converge exponentially with increasing resolution and at roughly the same rate. Each individual calculation samples and weights the configuration space wave function uniquely but all behave in a qualitatively similar manner. These results suggest that the method has great promise for similarly accurate treatment of few-particle systems.

PACS numbers: 31.15.ac,02.70.Jn,31.15.ag,03.65.Ge,02.60.Lj,02.30.Jr

*grabowski@lanl.gov

†Current Address: Computational Physics Group (CCS-2), Los Alamos National Laboratory, Mail Stop D413, Los Alamos, NM 87545, USA

‡chernoff@astro.cornell.edu

I. INTRODUCTION

This article develops the pseudospectral method as a numerical means of solving Schrödinger's equation for two-electron systems in terms of fully correlated wavefunctions. We test and validate the method on states of the helium atom, a system well-studied since the birth of quantum mechanics. The method achieves essentially arbitrary numerical precision and accuracy. Any such method which may be applied to a variety of problems (*e.g.* high-precision relativistic corrections, different interaction potentials, excitation levels, symmetries, etc.) without tinkering with or modifying the basis and which has direct, rigorous control of local errors serves as a complementary approach to the variational method. This work is a first step towards developing similarly capable tools for dealing with few-electron systems.

Methods based on the variational principle, in which the expectation value of the Hamiltonian is minimized with respect to the parameters of a trial wave function, are the most widely used techniques for finding approximate representations of the ground state and lowest excited states. The calculated energies are upper bounds to the exact energy. If one regards the best approximate wave function as first order accurate then the variationally determined energy eigenvalue is second order accurate. Small errors in the energy eigenvalue of a given state imply that the square of the wave function is accurate in the energy-weighted norm but not that the local wave function errors are also small. In practical terms, while the variational approach excels at determining energy eigenvalues it does not generally achieve comparable accuracy in quantum mechanical matrix elements formed from the wave function.

To achieve ever-more accurate energies and/or wave functions in the variational approach one must select a sequence of trial functions capable of representing the exact solution evermore closely. The choice of a good sequence entails more than a little art and intuition, especially for a nonstandard problem where one may have only a vague idea what the ultimate limit looks like. Calculations involving a sequence of increasing basis size n are said to converge exponentially if the errors are proportional to e^{-an} for some positive constant a. This most favorable outcome is achieved only if the basis can reproduce the analytic properties of the exact wave function. Otherwise, convergence is expected to be algebraic, *e.g.* $\propto n^{-2}$, or worse.

Recently, we applied pseudospectral methods to solve the nonrelativistic Schrödinger equation for helium and the negatively charged hydrogen ion with zero total angular momentum [1]. We found exponentially fast convergence of most quantities of interest including the energy eigenvalues, local energy errors (*i.e.* $(\hat{H}\Psi)/\Psi - E$ as a function of position) and Cauchy wave function differences. Only the error in the logarithmic derivative near the triple coalescence point had discernibly slower convergence, presumably due to the logarithmic contributions located there [2–4]. The key virtues of the pseudospectral approach were: no explicit assumptions had to be made about the asymptotic behavior of the wave function near cusps or at large distances, the Schrödinger equation was satisfied at all grid points, local errors decreased exponentially fast with increasing resolution, and no fine tuning was required.

In this article, we extend our previous work to higher angular momentum calculations and utilize the results to evaluate matrix elements for combinations of states. To be systematic, we consider two sorts of matrix elements: the dipole absorption oscillator strength (between an S and P state) and a wide range of expectation values of the ground state. All have been the subject of extensive investigation. Our main focus is on testing the pseudospectral method's capabilities by recalculating these quantities and comparing to effectively "exact" published results. We make no attempt to improve the accuracy of the best results in the literature.

The plan of the paper is as follows. The first four sections are largely background: §II provides an overview of the pseudospectral method; §III describes the two-electron atom, the Bhatia-Temkin coordinate system, the expansion of the wave function in this system and the form of the eigenvalue problem that this produces; §IV defines length, velocity and acceleration forms for the oscillator strength. §V gives a prescription for how to choose coordinates and subdomains for second order partial differential equations and outlines the special coordinate choices needed to deal with Coulomb singularities. §VI briefly describes the boundary conditions needed to properly solve the two-electron atom system. §VII presents convergence studies of energies, an oscillator strength, and expectation values. §VIII summarizes the capabilities and promise of the pseudospectral method.

II. THE PSEUDOSPECTRAL METHOD

Pseudospectral methods have proven success in solving systems of partial differential equations in a wide variety of fields including fluid dynamics [5], general relativity [6, 7], and quantum chemistry [8–16]. Some problems in one-electron quantum mechanics [17, 18] have been treated but only recently has the method been applied to the case of fully-correlated, multi-electron atoms [1]. Pseudospectral methods are discussed in some generality in Refs. [1, 7, 19–22].

The pseudospectral method is a grid-based finite difference method in which the order of the finite differencing is equal to the resolution of the grid in each direction. The grid points are located at the roots of Jacobi polynomials or their antinodes plus endpoints. In this article, the roots of Legendre polynomials are used. As the grid size increases it becomes more accurate than any fixed-order finite difference method. If a solution is smooth over an entire domain (or smooth in each subdomain) the pseudospectral method converges exponentially fast to the solution. A spectral basis expansion and a pseudospectral expansion of the same order are nearly equivalent, having differences that are exponentially small.

We define a natural and elegant set of bras and kets using the fundamental elements of the pseudospectral basis: let $|X^K\rangle$ be a position eigenstate corresponding to the Kth grid point and let $\langle X|\mathcal{C}_J\rangle$ be the multidimensional cardinal function (for details, see appendix A). The pseudospectral representation of the Hamiltonian is

$$\hat{H}_{PS} = \sum_{JK} |\mathrm{X}^K\rangle\langle \mathrm{X}^K|\hat{H}|\mathcal{C}_J\rangle\langle\mathcal{C}_J|, \tag{1}$$

where $\hat{H}$ is the full Hamiltonian operator. In practice, the matrix $\langle \mathrm{X}^K|\hat{H}_{PS}|\mathcal{C}_J\rangle$ is truncated and then diagonalized to find the energy eigenvalues. When the wave function is represented by a pseudospectral expansion the eigenvectors are simply the function values at the grid points. In a spectral representation, by contrast, the eigenvectors are coefficients of basis functions. It is often more convenient and efficient to work with the local wave function values directly.

III. THE NONRELATIVISTIC TWO-ELECTRON ATOM

In the infinite-nuclear-mass and nonrelativistic approximations the Hamiltonian is

$$\hat{H}_0 = \frac{1}{2}(p_1^2 + p_2^2) + \hat{V}, \tag{2}$$

where $\mathbf{p}_{1,2}$ are the momentum operators of the two electrons and the potential is

$$\hat{V} = -\frac{Z}{r_1} - \frac{Z}{r_2} + \frac{1}{r_{12}}, \tag{3}$$

where Z is the nuclear charge, and r_1, r_2, and r_{12} are the magnitudes of the vectors pointing from the nucleus to each electron and of the vector pointing from one electron to the other, respectively. Here and throughout this article, atomic units are used.

The full wave functions are six-dimensional. For S states, Hylleraas [23] showed that the non-trivial part of the wave function could be written in terms of three internal coordinates. Typical choices for these coordinates are r_1, r_2, and r_{12}. Alternatively, r_{12} may be replaced by θ_{12}, the angle between the two electrons. The S states are independent of the remaining three coordinates that describe the orientation of the triangle with vertices at the two electrons and nucleus.

The situation for states of general angular momentum is more complicated. Bhatia and Temkin [24] introduced a particular set of Euler angles $\{\Theta, \Phi, \Psi\}$ to describe the triangle's orientation. They defined[1] a set of generalized spherical harmonics $D^{\nu}_{\kappa lm}$ which are eigenstates of operators for the total angular momentum, its z component, total parity ($\{\mathbf{r}_1, \mathbf{r}_2\} \rightarrow \{-\mathbf{r}_1, -\mathbf{r}_2\}$), and exchange ($\hat{\mathcal{E}}_{12} = \mathbf{r}_1 \leftrightarrow \mathbf{r}_2$). In terms of these functions, the wave function can be written as

$$\psi_{lms}[\mathbf{r_1}, \mathbf{r_2}] = \sum_{\nu=0}^{1} {\sum_{\kappa=\nu}^{l}}' g^{\nu}_{\kappa ls}[r_1, r_2, \theta_{12}] D^{\nu}_{\kappa lm}[\Theta, \Phi, \Psi], \tag{4}$$

where the prime on the sum means that κ is restricted to even or odd numbers if parity is even or odd, respectively, and $g^{\nu}_{\kappa ls}$ is a real function of the internal coordinates. The convenience of the Bhatia and Temkin [24] coordinate choice is most evident in how one

[1] The symbols differ slightly from those of Bhatia and Temkin [24] so that the equations can be written compactly. Our $D^0_{\kappa lm}$ ($D^1_{\kappa lm}$) is $\mathcal{D}_l^{(m,\kappa)+}$ ($\mathcal{D}_l^{(m,\kappa)-}$) in Ref. [24], where l and m are angular momentum and magnetic quantum numbers, κ is the angular momentum about the body-fixed axis of rotation and $\pm$ labels combinations of the vector spherical harmonics.

imposes total antisymmetry of the wave function. The spin singlet (triplet) must have a symmetric (antisymmetric) spatial wave function. The properties of the $D^{\nu}_{\kappa lm}$ functions reduce this requirement to

$$\hat{\mathcal{E}}_{12} g^{\nu}_{\kappa ls} = (-1)^{\nu+\kappa+l+s} g^{\nu}_{\kappa ls}. \tag{5}$$

The total antisymmetry of a wave function with given parity, l, m and s follows by imposing the above requirement under $r_1 \leftrightarrow r_2$ on each radial function for each ν and κ. Note that $(-1)^{\kappa+l+s}$ is fixed directly by the wave function's parity, l and s. The same requirement applies to both singlet and triplet states up to the difference in the value of s.

The full six-dimensional Schrödinger equation for given l, s, parity, and any m yields l or $l+1$ (depending on these quantum numbers) coupled three-dimensional equations for $g^{\gamma}_{\kappa ls}$. The indices for g satisfy $\gamma = 0$ or 1 and $0 \leq \kappa \leq l$ with even or odd κ for even or odd parity, respectively. The equations are

$$0 = (\hat{H}_S - E) g^{\gamma}_{\kappa ls} + \sum_{\nu=0}^{1} \sum_{n=-1}^{1} \hat{H}^{\gamma}_{\nu\kappa n} g^{\nu}_{\kappa+2n,l,s}, \tag{6}$$

where $\hat{H}_S$ is the part of the Hamiltonian operator that survives for S states. The summation enumerates couplings with $\gamma \neq \nu$ and/or different κ as well as terms that are intrinsic to non-S-states. Appendix B gives the explicit forms of the operators $\hat{H}_S$ and $\hat{H}^{\gamma}_{\nu\kappa n}$ and appendix C 1 shows how to set up Eq. 6 as a matrix problem. The notation above might obscure the fact that the matrices associated with states of higher angular momentum are larger and more complicated than those for lower momentum so we simply point out that treating P states requires matrices roughly four times as large as S states.

IV. THE OSCILLATOR STRENGTH

The length, velocity and acceleration forms for the oscillator strength [25] are

$$f^{l}_{ij} = \frac{2}{3}(E_j - E_i)|\langle j|\mathbf{R}|i\rangle|^2 \tag{7}$$

$$f^{v}_{ij} = \frac{2}{3}\frac{1}{E_j - E_i}|\langle j|\mathbf{P}|i\rangle|^2 \tag{8}$$

$$f^{a}_{ij} = \frac{2}{3}\frac{1}{(E_j - E_i)^3}\left|\langle j\left|\mathbf{A}\right|i\rangle\right|^2, \tag{9}$$

where E_i and E_j are the energies of the initial and final states and $\mathbf{R}$, $\mathbf{P}$, and $\mathbf{A}$ are the total position, momentum, and acceleration operators, respectively. Appendix D presents

explicit expressions for f used in the calculations.

If the wave functions, energies, and operators were exact, all three forms would give identical results. However, in a numerical calculation the agreement may be destroyed whenever the operator commutator rule

$$\mathbf{P} = i[\hat{H}_0, \mathbf{R}] \tag{10}$$

is violated. Approximations to the operators ($\hat{H}_0$, $\mathbf{P}$, or $\mathbf{R}$) and to the initial and final eigenstates are possible sources of error. Good agreement between the three forms at a fixed resolution has sometimes been taken to be an indication of an accurate answer. Such agreement is ultimately necessary as resolution improves but the closeness of the agreement is insufficient to infer the accuracy at a fixed resolution [25, 26]. A more stringent approach involves two steps: first, for each form check that the matrix element converges with resolution or basis size and, second, that the converged answers for different forms agree.

This article exemplifies the capabilities of the pseudospectral approach by evaluating the $1^1\mathrm{S} \rightarrow 2^1\mathrm{P}$ oscillator strength, a physical regime in which strong electron correlations are paramount.

V. VARIABLES AND DOMAINS

A. General prescription

The choices of coordinates and computational subdomains are important aspects of the application of the pseudospectral method. Special treatment is needed whenever the solution is non-smooth – otherwise the property of exponential convergence is lost. The Coulomb singularities are, of course, generic in atomic physics applications and lead to cusps and other discontinuities. Ref. [1] describes the need to use a radial-like coordinate about each two-particle singularity of helium-like atoms. Here we generalize that prescription and discuss in more depth the treatment of multiple singularities.

The ordinary differential equation

$$\left(\frac{d^2}{d\mathrm{X}^2} + \frac{p_a[\mathrm{X}]}{\mathrm{X} - a} \frac{d}{d\mathrm{X}} + \frac{q_a[\mathrm{X}]}{(\mathrm{X} - a)^2} \right) f = 0 \tag{11}$$

with $p_a[\mathrm{X}]$ and $q_a[\mathrm{X}]$ analytic at $\mathrm{X} = a$ has a regular singular point at $\mathrm{X} = a$. The basic theory of ordinary differential equations (ODE's) [27] states that f has at least one

Frobenius-type solution about $\mathrm{X} = a$ of the form

$$f[\mathrm{X}] = (\mathrm{X} - a)^{t_a} \sum_{n=0}^{\infty} c_n (\mathrm{X} - a)^n, \tag{12}$$

where the coefficients c_n can be derived by directly plugging into Eq. 11 and t_a is the larger of the two solutions to the indicial equation

$$t_a(t_a - 1) + p_a[a]t_a + q_a[a] = 0. \tag{13}$$

Exponential convergence of the pseudospectral method for a differential equation of the form of Eq. 11 requires t_a be a non-negative integer. This must hold at each singularity a in the domain (as well as all other points).[2]

A simple example is the Schrödinger equation for a hydrogenic atom expressed in spherical coordinates $\{\mathrm{X}_1, \mathrm{X}_2, \mathrm{X}_3\} = \{r, \theta, \phi\}$. The radial part of the full wave function $R_{nl}[r]$ satisfies

$$\left(\frac{d^2}{dr^2} + \frac{2}{r}\frac{d}{dr} - \frac{l(l+1) - 2Zr - 2Er^2}{r^2} \right) R_{nl} = 0. \tag{14}$$

A comparison with Eq. 11 yields $p_0[0] = 2$ and $q_0[0] = -l(l+1)$, which gives $t_0 = l$, the well known result for hydrogenic wave functions. The reduction of the partial differential equation (PDE) to an ODE having non-negative integer t_0 tells us that spherical coordinates are a good choice for solving hydrogenic wave functions using pseudospectral methods. A bad choice would be Cartesian coordinates $\{\mathrm{X}_1, \mathrm{X}_2, \mathrm{X}_3\} = \{x, y, z\}$. The ground state has the form

$$\psi \propto e^{-Z\sqrt{x^2+y^2+z^2}}. \tag{15}$$

This solution has a discontinuity in its first derivatives at $x = y = z = 0$:

$$\lim_{x,y,z \to 0^+} \frac{\partial \psi}{\partial x, y, z} \neq \lim_{x,y,z \to 0^-} \frac{\partial \psi}{\partial x, y, z}. \tag{16}$$

Other solutions have a discontinuity of first or higher derivatives at the same point. The pseudospectral method would not handle these well and convergence would be limited to being algebraic.

An arbitrary second order PDE may have singularities that occur on complicated hypersurfaces of different dimensionality. Deriving the analytic properties of a solution near

[2] The full class of one dimensional problems for which pseudospectral methods converge exponentially fast is larger than this description. The method needs the solution to be smooth which is a weaker statement than that it be analytic. This distinction is not material for the singular points discussed here.

such a surface is a daunting task. The general idea is to seek a coordinate system such that the limiting form of the PDE near the singularity looks like an ODE of the sort that pseudospectral methods are known to handle well.

In an n-dimensional space, assume the singularity lies on an $(n-1)$-dimensional surface.[3] First, seek a coordinate system such that the surface occurs at $\mathrm{X}_i = a$. Second, focusing on X_i, seek coordinates so that it is possible to rewrite the PDE in the form

$$\left(\frac{\partial^2}{\partial {\mathrm{X}_i}^2} + \frac{\hat{P}_a[\mathrm{X}]}{\mathrm{X}_i - a} \frac{\partial}{\partial \mathrm{X}_i} + \frac{\hat{Q}_a[\mathrm{X}]}{(\mathrm{X}_i - a)^2} \right) f = 0 \tag{17}$$

where $\hat{P}_a$ and $\hat{Q}_a$ are linear second order differential operators that do not include derivatives with respect to X_i and $\mathrm{X} = \{\mathrm{X}_1, \mathrm{X}_2, \ldots\}$. Finally, seek coordinates such that $\hat{P}_a$ and $\hat{Q}_a$ are analytic with respect to X_i at a.

Unfortunately, even if one succeeds in finding such a coordinate system, the theorem of ODEs does not generalize to PDEs, i.e. there is no guarantee that f is analytic near a. A celebrated example is exactly the problem of concern here, i.e. the Schrödinger equation for two-electron atoms. Three coordinates are needed to describe the S state. In hyperspherical coordinates ($\{X_1, \ldots\} = \{\rho, \ldots\}$ where $\rho = \sqrt{r_1^2 + r_2^2}$), Schrödinger's equation matches the form of Eq. 17 for $\mathrm{X}_1 = \rho$ and $a = 0$. This is the triple coalescence point, a point singularity in the three-dimensional subspace spanned by the coordinates r_1, r_2, and r_{12}. The electron-nucleus and electron-electron singularities (two-body coalescence points) are one-dimensional lines in this subspace that meet at $\rho = 0$. Bartlett [2] proved that no wave function of the form

$$\psi = \sum_{n=0}^{\infty} A_n \rho^n, \tag{18}$$

where A_n is an analytic function of the remaining variables will satisfy the PDE. Fock's form for the solution [3, 4] is

$$\psi = \sum_{n=0}^{\infty} \sum_{m=0}^{\lfloor n/2 \rfloor} B_{nm} \rho^n (\log \rho)^m, \tag{19}$$

where B_{nm} is an analytic function of the remaining variables. The presence of the $\log \rho$ terms in the wave function is an important qualitative distinction between a solution having two- and three-body coalescence points.

[3] A singularity of dimension less than $n-1$ is treated as a limiting case. For example, in the previous example with spherical coordinates the Coulomb singularity at $r = 0$ is regarded as the limit of a two-dimensional sphere whose radius approaches zero.

Some properties of the solution near $\rho = 0$ have been reviewed in our previous article [1]. For example, Myers *et al.* [28] showed that the logarithmic terms allow the local energy $(\hat{H}\psi)/\psi$ near $\rho = 0$ to be continuous. Despite this property, they have only a slight effect on the convergence of variational energies [29]. By many measures of error the triple coalescence point does not affect pseudospectral calculations until very high resolutions [1].

As a point of principle, however, no simple coordinate choice can hide the problems that occur at the triple coalescence point, and no special method for handling this singularity is given here. Our rule of thumb is the following: coordinates are selected so that the singularity may be described by $X_i = a$ with $\hat{P}_a$ and $\hat{Q}_a$ satisfying

$$\hat{P}_a = \sum_{n=0}^{\infty} (\mathrm{X}_i - a)^n \hat{p}_{an} \tag{20}$$

$$\hat{Q}_a = \sum_{n=0}^{\infty} (\mathrm{X}_i - a)^n \hat{q}_{an}, \tag{21}$$

in a neighborhood about $\mathrm{X}_i = a$. Here, $\hat{p}_{an}$ and $\hat{q}_{an}$ are linear differential operators not containing X_i or its derivatives. If more than one singularity is within a subdomain, this condition must be satisfied for each of them.

B. For the two-electron atom

The singularities of the Hamiltonian, given in detail in Appendix B, are of two types. The physical singularities at r_1, r_2, and $r_{12} = 0$ were explored in Ref. [1]. One of the essential virtues of hyperspherical coordinates is that $\rho \neq 0$ implies these coalescences have separate neighborhoods. Therefore, the prescription is to seek separate coordinates satisfying eqs. 20 and 21 in the vicinity of each singularity.

There are also coordinate singularities at $\theta_{12} = 0$ and π, which correspond to collinear arrangements of the two electrons and nucleus. These singularities were completely absent in our previous treatment of S states [1]. For more general states, the wave functions are no longer analytic with respect to the coordinates C and B used in that article. So we use the coordinates θ_{12} and β_{12} instead, where $C = -\cos\theta_{12}$ and $B = -\cos\beta_{12}$. All other coordinates are identical. Eqs. 20 and 21 are then satisfied by choosing the same subdomains as in Ref. [1]. Fig. 1 illustrates the layout of these three subdomains at fixed ρ.

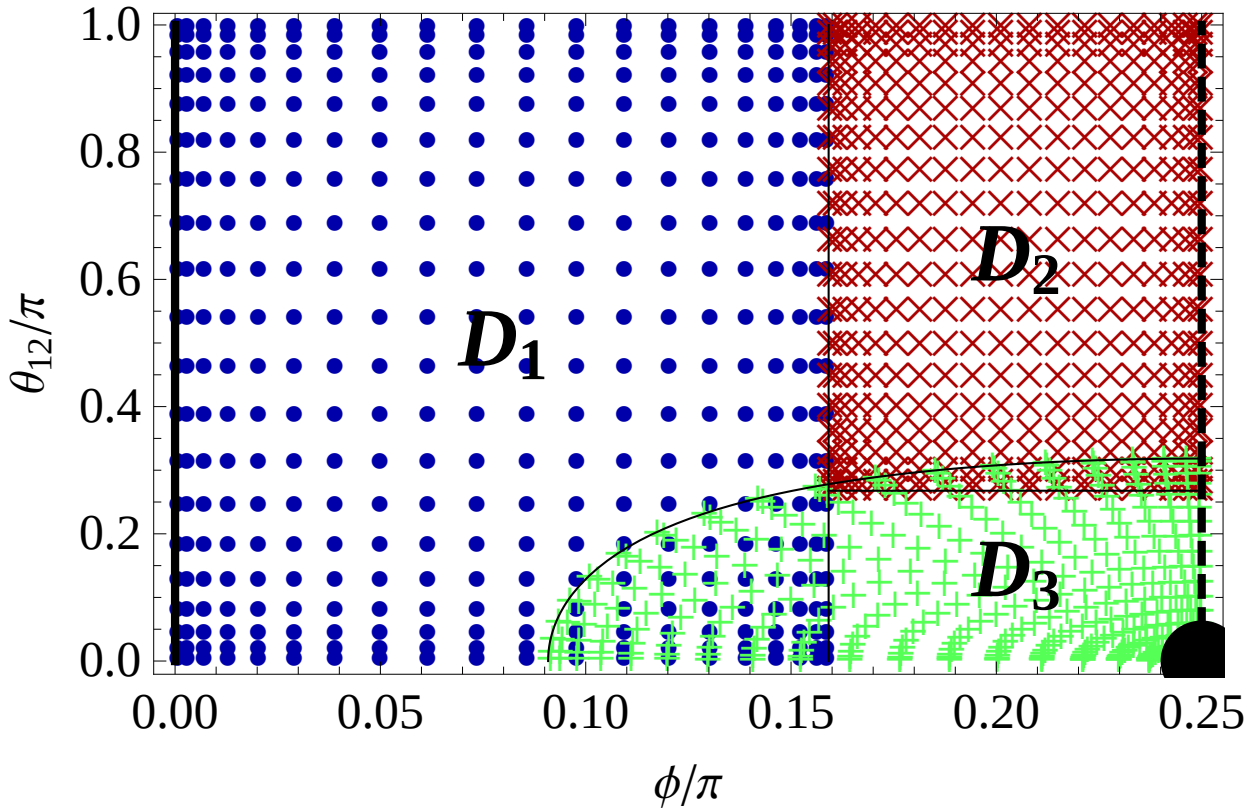

FIG. 1: (Color online). This is the arrangement of grid points of the three domains at a constant value of ρ in ϕ and θ_{12} coordinates for $n = 20$. Note that the point density becomes larger at the boundary of each subdomain and that no grid points sit on the Coulomb singularities. The blue circles, red crosses, and green pluses belong to domains D_1, D_2, and D_3, respectively. D_1 and D_2 are rectangular domains, while D_3 has the curved boundary in ϕ, θ_{12} coordinates but is rectangular in ζ, β_{12} coordinates. The electron-proton singularity occurs on the left side (solid line at $\phi = 0$). The entire line corresponds to one physical point. The electron-electron singularity occurs at the lower right hand corner (solid disk at $\phi = \pi/4, \theta_{12} = 0$). A line of symmetry falls on the right side (dashed line at $\phi = \pi/4$ where $r_1 = r_2$).

VI. BOUNDARY CONDITIONS

The internal boundary conditions are the same as in Ref. [1]. Briefly, we enforce continuity of the wave function at all subdomain boundaries and continuity of the normal derivative wherever two subdomains barely touch.

The symmetry due to electron exchange is a little more complicated because each wave

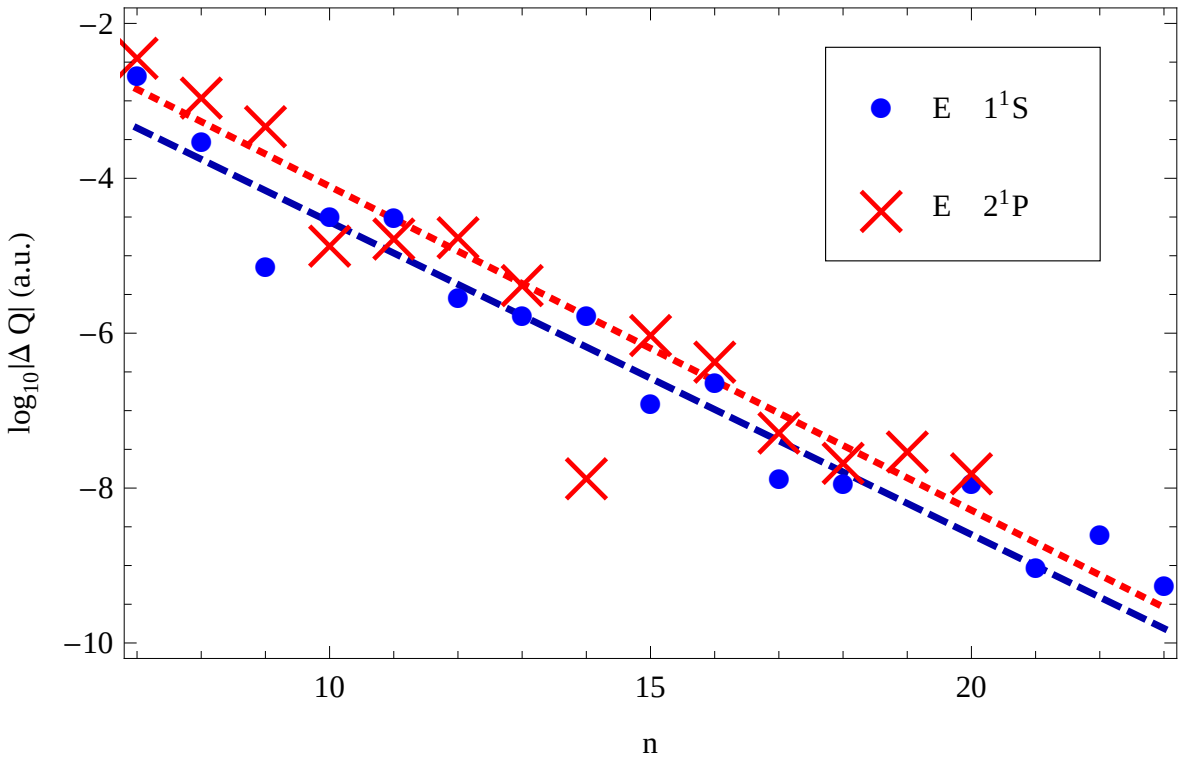

FIG. 2: (Color online). The logarithm base 10 of the energy error (ΔQ) of both the lowest energy S state and P state of helium. The dark blue circles are for the 1^1S state and the light red crosses for the 2^1P state with dashed blue and dotted red fits, respectively (see Tab. I).

function can require multiple three-dimensional functions for its evaluation (see Eq. 4). The conditions

$$0 = \begin{cases} \left.\frac{\partial g^{\nu}_{\kappa ls}}{\partial \phi}\right|_{\phi=\pi/4} = \left.\frac{\partial g^{\nu}_{\kappa ls}}{\partial \beta_{12}}\right|_{\beta_{12}=\pi/2} & \text{if } \xi \text{ is even} \\ g^{\nu}_{\kappa ls}|_{\phi=\pi/4} = g^{\nu}_{\kappa ls}|_{\beta_{12}=\pi/2} & \text{if } \xi \text{ is odd} \end{cases}, \tag{22}$$

where $\xi = \nu + \kappa + l + s$, give the required symmetry.

VII. RESULTS

A. The energy and oscillator strength

Figure 2 shows the energy errors for the 1^1S and 2^1P states of helium. Here and throughout the results section the high precision values of Drake [30] are taken to be exact. The energy error for both states decreases exponentially with resolution. Convergence for the S state is similar to that reported in Ref. [1] with slight differences related to a different

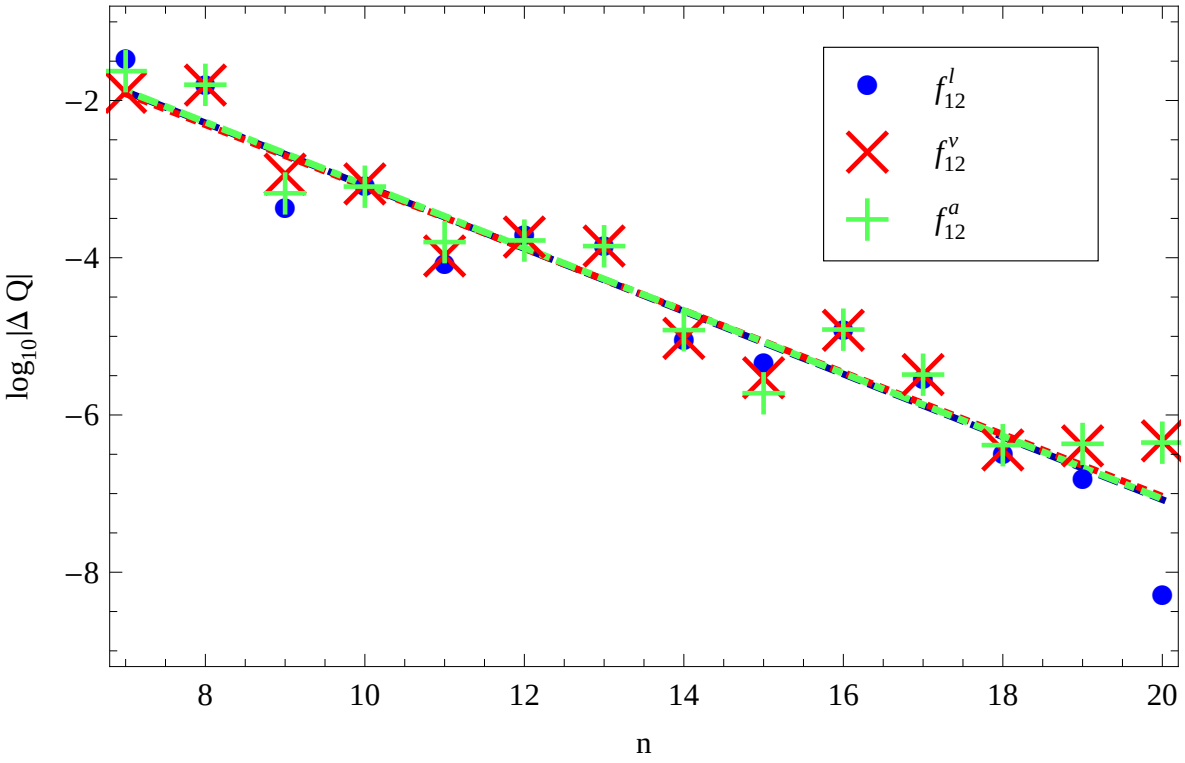

FIG. 3: (Color online). The logarithm base 10 of the error (ΔQ) in the oscillator strength of the $1^1\mathrm{S} \rightarrow 2^1\mathrm{P}$ transition of helium. The dark blue circles are for the length form, the light red crosses are for the velocity form, and the green pluses for the acceleration form with dashed blue, dotted red, and dot-dashed green fits, respectively (see Tab. I).

choice of coordinates. The current calculation extends to basis size $n = 23$ for S states and $n = 20$ for P states instead of $n = 14$ for only S states in Ref. [1].

A common feature of the energy convergence and the convergence of all other quantities in this article is they are non-monotonic. This method is not variational, so there is no reason to expect monotonic convergence. Calculated quantities can fall above or below their actual value, with error quasi-randomly determined by the exact grid point locations. The jumps decrease in magnitude as the resolution is increased.

As described in Sec. IV, there are three commonly used calculational forms for the oscillator strength. The length, velocity, and acceleration forms depend most strongly on the value of the wave function at positions in configuration space corresponding to large, medium, and small separations. Sometimes the relative errors are used to infer where the wave function is more or less accurate. It has been observed that for most variational calculations, the

acceleration form tends to be much less accurate than the other two forms, suggesting errors in the wave function at small separation that have little effect on the variational energy. The length and velocity forms give results of roughly comparable accuracy.

The oscillator strength of the $1^1\mathrm{S} \rightarrow 2^1\mathrm{P}$ transition was calculated using all three forms and Fig. 3 displays the errors. Here, all three forms give roughly the same results. At most resolutions the points lie nearly on top of one another and their fits are indistinguishable, indicating the wave function errors for small, medium, and large separations have roughly equal contributions to the numerically calculated oscillator strength. This may be due to the pseudospectral method's equal treatment of all parts of configuration space.

It should be noted that the value used as the exact value [30] is given to seven decimal places. Consequently, the errors inferred for the highest resolution calculations in Fig. 3 are not too precise. Aside from testing calculational methods, as we do here, there is little practical need for additional digits since a host of other effects including finite nuclear mass, relativistic, and quadrupole corrections would confound any hypothetical, experimental measurement of the oscillator strength to this precision. Actual experiments struggle to obtain two percent precision [31], an error larger than these effects.

As pointed out by Schiff *et al.* [26] and reviewed by Hibbert [25], the assumption that using the differences between the oscillator strength values from the different forms as a measure of the accuracy is not valid. Agreement is necessary but not sufficient. They suggest comparing calculated and extrapolated values. This latter procedure is not straightforward for a pseudospectral method with non-monotonic convergence. We present a similar suitable check. Fig. 4 shows the average and standard deviation of the error for the three forms as a function of resolution. The standard deviation is about an order of magnitude (with a large scatter about that factor of ten) less than the average error at low and moderate resolutions but the trend lines suggest that the standard deviation may be approaching the average at the higher resolutions. A possible explanation is that the calculation at the highest resolutions is starting to become sensitive to the wave function truncation (see appendix C 2). This destroys the expected equality between the forms and each form converges to its own incorrect asymptotic value. The individual errors and the standard deviation become comparable. So at $n = 20$, we assume the standard deviation and total error are equal and get a value for the oscillator strength of 0.27616499(27) which compares favorably to Drake's 0.2761647 [30].

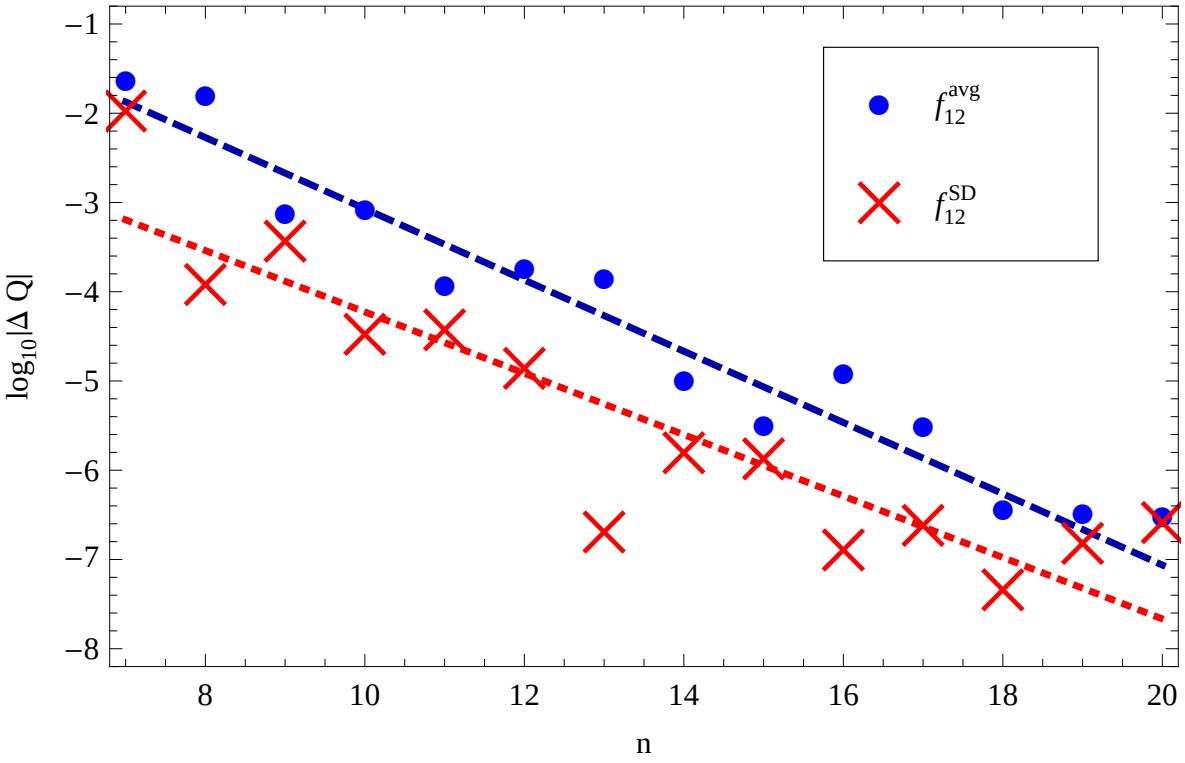

FIG. 4: (Color online). The logarithm base 10 of the error (ΔQ) in the average of the length, velocity, and acceleration forms of the oscillator strength (dark blue circles) and their standard deviation (light red crosses) for the $1^1\mathrm{S} \rightarrow 2^1\mathrm{P}$ transition of helium, with dashed blue and dotted red fits, respectively (see Tab. I).

TABLE I: The fit parameters to all the convergence plots of quantities Q in this section.

Q	Figure	A	β
$E(1^1\mathrm{S})$	2	2.5×10^{-9}	0.40
$E(2^1\mathrm{P})$	2	5.2×10^{-9}	0.42
f_{12}^{l}	3	8.4×10^{-8}	0.40
f_{12}^{v}	3	9.2×10^{-8}	0.39
f_{12}^{a}	3	8.6×10^{-8}	0.40
f_{12}^{avg}	4	8.7×10^{-8}	0.40
f_{12}^{SD}	4	2.2×10^{-8}	0.34

TABLE II: The highest resolution values and fit parameters to the convergence data of many expectation values.

Q	Value (n=23)	A	β
$\langle r_1^2 \rangle$	1.193482995298	3.3×10^{-11}	0.54
$\langle r_{12}^2 \rangle$	2.516439313796	1.2×10^{-10}	0.53
$\langle \mathbf{r_1} \cdot \mathbf{r_2} \rangle$	-0.064736661600	4.9×10^{-11}	0.47
$\langle r_1 \rangle$	0.929472295020	1.2×10^{-11}	0.48
$\langle r_{12} \rangle$	1.422070255931	7.5×10^{-11}	0.46
$\langle 1/r_1 \rangle$	1.688316800531	1.1×10^{-10}	0.37
$\langle 1/r_{12} \rangle$	0.945818448516	1.2×10^{-10}	0.37
$\langle 1/r_1^2 \rangle$	6.017408866115	7.1×10^{-10}	0.36
$\langle 1/r_{12}^2 \rangle$	1.464770922396	3.1×10^{-10}	0.38
$\langle 1/r_1 r_2 \rangle$	2.708655473629	3.9×10^{-10}	0.37
$\langle 1/r_1 r_{12} \rangle$	1.920943921111	2.6×10^{-10}	0.37
$\langle \delta(r_1) \rangle$	1.810429318201	2.4×10^{-10}	0.36
$\langle \delta(r_{12}) \rangle$	0.106345370527	6.5×10^{-11}	0.36
$\langle \mathbf{p}_1 \cdot \mathbf{p}_2 \rangle$	0.159069476264	2.4×10^{-10}	0.39
$\langle \hat{H}_{\mathrm{OO}} \rangle / \alpha^2$	-0.139094692705	4.3×10^{-10}	0.38

All convergence data were fit to functions of the form $\Delta Q = A \times 10^{-\beta(n-20)}$ using the same procedure as in Ref. [1]. Because of uncertainty in the errors for the largest resolutions ($n = 19$ and $n = 20$) these points were not used in the fits of f_{12}^l, f_{12}^v, f_{12}^a, and f_{12}^{avg}. The β parameter, which corresponds to the slope of the fits in the convergence graphs is roughly the same for all fits, with the exception of the standard deviation of the oscillator strength forms. This behavior is consistent with our discussion of errors in the previous paragraph.

B. Expectation values

We calculated many different expectation values to emphasize the pseudospectral method's ability to treat many observables with the same exponential accuracy as the energy. These expectation values sample different parts of configuration space differently and

some involve derivatives and Dirac delta functions. All expectation values were calculated at the same set of resolutions ($n = 7 - 23$) as the energy. As in the previous subsection, these data were fit to functions of the form $A \times 10^{-\beta(n-23)}$ (Note the use of 23 instead of 20 because $n = 23$ was the highest resolution used for S states.) using the same procedure as in Ref. [1]. The fit parameters are shown in Tab. II. The most striking feature is how similar the magnitudes of the errors are at $n = 23$. The exponential parameter β is higher for the first few expectation values. This difference is due to those operators more strongly weighing the relatively inexact low resolution wave function values at large distances. As resolution is increased, this discrepancy goes away. Indeed, as one increases resolution one increases the accuracy of all expectation values or oscillator strengths by roughly the same amount.

VIII. CONCLUSIONS

We developed a general prescription for choosing coordinates and subdomains for a pseudospectral treatment of partial differential equations in the presence of physical and coordinate-related singularities. It accounts for two-body but not three-body coalescences. We solved Schrödinger's equation for helium to determine the fully correlated wave function.

The method attained exponentially fast convergence for a wide selection of expectation values and matrix elements like the oscillator strength. Variational approaches minimize energy-weighted errors but generally do not yield comparable results for other operators. So it is noteworthy that the pseudospectral method produced errors and convergence rates that were very similar for all the quantities studied including energy. The pseudospectral representation of the wave function (via Eqs. 4 and A5) is completely analogous to a variationally derived form, i.e. it is a complete configuration space representation.

These results also represent a generalization of our previous calculations from the ground S state to the lowest energy P state. Application to higher energies and/or higher angular momenta is straightforward but more computationally expensive.

The oscillator strength of the helium $1^1\mathrm{S} \rightarrow 2^1\mathrm{P}$ transition was calculated to about the same accuracy as the most accurate value in the literature [30] and was found to agree to the expected precision.

Several aspects of the approach suggest it should be applicable for few electron systems.

No fine tuning was done to improve convergence other than ensuring non-analytic behavior was treated properly. The numerical method we developed was capable of solving the large matrix problems with modest computational resources. The prescription for choosing coordinates and subdomains is applicable to problems with two-particle singularities. Other problems with Coulomb singularities can now be tackled with the pseudospectral method.

Appendix A: Pseudospectral representation of a function

The eigenvector of a pseudospectral matrix gives the values of a wave function at a discrete set of points. Often it is useful to have values off the grid. In this appendix, we show how to interpolate to the full exponential accuracy of the method.

Let $\{\mathrm{X}^k\}_{k=1,2,\ldots N}$ be the roots of an Nth order Jacobi polynomial enumerated by k. Let X stand for an arbitrary coordinate value in the dimension of interest. Define the one dimensional cardinal functions

$$C_j[\mathrm{X}] = \prod_{\substack{k=1 \\ k\neq j}}^{N} \frac{\mathrm{X} - \mathrm{X}^k}{\mathrm{X}^j - \mathrm{X}^k} \tag{A1}$$

and note the relation

$$C_j[\mathrm{X}^k] = \delta_j^k \tag{A2}$$

follows. Now let the n_d-dimensional grid be the tensor product of the individual, one dimensional coordinate grids labeled by $X_{(i)}$ for $i = 1$ to n_d. The corresponding cardinal functions are

$$\mathcal{C}_J[\mathrm{X}] = \prod_{i=1}^{n_d} C_{j_{(i)}}[\mathrm{X}_{(i)}], \tag{A3}$$

where subscript $J = \{j_{(1)}, j_{(2)}, \ldots, j_{(n_d)}\}$ and unadorned $\mathrm{X} = \{\mathrm{X}_{(1)}, \mathrm{X}_{(2)}, \ldots, \mathrm{X}_{(n_d)}\}$. These multi-dimensional Cardinal functions have the property

$$\mathcal{C}_J[\mathrm{X}^K] = \delta_J^K, \tag{A4}$$

where the grid point $\mathrm{X}^K = \{\mathrm{X}_{(1)}^{k_1}, \mathrm{X}_{(2)}^{k_2}, \ldots, \mathrm{X}_{(n_d)}^{k_{n_d}}\}$. They form a basis in the sense that a general function f can be written

$$f[\mathrm{X}] = \sum_J f[\mathrm{X}^J]\mathcal{C}_J[\mathrm{X}], \tag{A5}$$

where $f[\mathrm{X}^J]$ is a pseudospectral coefficient ("pseudo" because it is more easily identified as the function value at the grid point).

Appendix B: Bhatia and Temkin Hamiltonian

Bhatia and Temkin [24] derived and we checked the following explicit expressions that make up the Hamiltonian in their three-three splitting:

$$\hat{H}_S = -\frac{1}{2}\sum_{i=1}^{2}\frac{1}{r_i^2}\left(\frac{\partial}{\partial r_i}r_i^2\frac{\partial}{\partial r_i} + \frac{1}{\sin\theta_{12}}\frac{\partial}{\partial\theta_{12}}\sin\theta_{12}\frac{\partial}{\partial\theta_{12}}\right) + \hat{V} \tag{B1}$$

$$\hat{V} = -\frac{Z}{r_1} - \frac{Z}{r_2} + \frac{1}{r_{12}} \tag{B2}$$

$$\hat{H}^{\gamma}_{\nu,\kappa,-1} = (1-\delta_{0\kappa}-\delta_{1\kappa}+(-1)^{\nu}\delta_{2\kappa})h^{\gamma}_{\nu}B_{l\kappa,-1}\begin{cases}\cot\theta_{12} & \text{if } \nu=\gamma\\ (-1)^{\nu} & \text{if } \nu\neq\gamma\end{cases} \tag{B3}$$

$$\hat{H}^{\gamma}_{\nu\kappa 0} = h^{\gamma}_{\nu}\begin{cases}2\frac{l(l+1)-\kappa^2}{\sin\theta_{12}}+\kappa^2\sin\theta_{12}-\gamma\cot\theta_{12}l(l+1)\delta_{1\kappa} & \text{if } \nu=\gamma\\ \nu\kappa(2\cos\theta_{12}+4\sin\theta_{12}\frac{\partial}{\partial\theta_{12}})-l(l+1)\delta_{1\kappa} & \text{if } \nu\neq\gamma\end{cases} \tag{B4}$$

$$\hat{H}^{\gamma}_{\nu\kappa 1} = (1-\nu\delta_{0\kappa})h^{\gamma}_{\nu}B_{l,\kappa+2,1}\begin{cases}\cot\theta_{12} & \text{if } \nu=\gamma\\ (-1)^{\gamma} & \text{if } \nu\neq\gamma\end{cases} \tag{B5}$$

$$h^{\gamma}_{\nu} = \frac{1}{8\sin\theta_{12}}\left(\frac{1}{r_2^2}+\frac{\nu\gamma}{r_1^2}\right) \tag{B6}$$

$$B_{l\kappa n} = (1+\delta_{2\kappa}(\sqrt{2}-1))^n\sqrt{(l-\kappa+1)(l-\kappa+2)(l+\kappa)(l+\kappa-1)}. \tag{B7}$$

These operators are used in Eq. 6.

Appendix C: Matrix methods

1. Formalism

To solve for the wave function with given parity, l and s and any m, one must calculate the values of $g^{\nu}_{\kappa ls}$ for each κ and ν that enters the summation in Eq. 4. In this section we suppress writing l, s and m indices; only ν and κ will appear explicitly. There are two types of conditions which must be satisfied: the Schrödinger equation and the boundary conditions.

The κ values of interest are κ_m, the minimum value, κ_m+2, ... up to κ_M, the maximum value. The minimum and maximum values depend upon parity, l and ν (for notational

clarity omitted). The minimum κ is

$$\kappa_m = \nu + \frac{1}{2}(1 - (-1)^\nu k) \tag{C1}$$

and the maximum is

$$\kappa_M = 2\left\lfloor \frac{l}{2} \right\rfloor - \frac{(-1)^l}{2}(1-k), \tag{C2}$$

where $k = 1$ ($k = -1$) for even (odd) parity.

Let g^ν_κ stand for all the grid point values for a given ν and κ. Assemble these in a column vector form that enumerates the full set of κ for a fixed ν

$$g^\nu = \begin{pmatrix} g^\nu_{\kappa_m} \\ g^\nu_{\kappa_m+2} \\ \vdots \\ g^\nu_{\kappa_M} \end{pmatrix}. \tag{C3}$$

The length of this column vector is $\tilde{l} = 1 + (\kappa_M - \kappa_m)/2$, which takes on the values $\lfloor l/2 \rfloor$ or $\lceil l/2 \rceil$, so the size of the matrix problem increases linearly with l.

The Schrödinger equation can be represented in matrix form:

$$\begin{pmatrix} H^0_0 + (H_S - E)\mathbf{1} & H^0_1 \\ H^1_0 & H^1_1 + (H_S - E)\mathbf{1} \end{pmatrix} \begin{pmatrix} g^0 \\ g^1 \end{pmatrix} = 0, \tag{C4}$$

where E is the energy, H_S is the S-wave part and the H^γ_ν's are the non-S-wave parts of the Hamiltonian, and $\mathbf{1}$ is the identity matrix. H^γ_ν and $\mathbf{1}$ are square matrices with dimensions $\tilde{l} \times \tilde{l}$. Explicitly, H^γ_ν is the tridiagonal matrix

$$H^\gamma_\nu = \begin{pmatrix} H^\gamma_{\nu,\kappa_m,0} & H^\gamma_{\nu,\kappa_m,1} & 0 & \cdots & 0 \\ H^\gamma_{\nu,\kappa_m+2,-1} & H^\gamma_{\nu,\kappa_m+2,0} & H^\gamma_{\nu,\kappa_m+2,1} & \ddots & \vdots \\ 0 & H^\gamma_{\nu,\kappa_m+4,-1} & H^\gamma_{\nu,\kappa_m+4,0} & \ddots & 0 \\ \vdots & \ddots & \ddots & \ddots & H^\gamma_{\nu,\kappa_M-2,1} \\ 0 & \cdots & 0 & H^\gamma_{\nu,\kappa_M,-1} & H^\gamma_{\nu,\kappa_M,0} \end{pmatrix}. \tag{C5}$$

The third subscript on the $H^\gamma_{\nu\kappa n}$ labels the coupling of the individual g functions in κ. For the S and P states calculated in this article, H^γ_ν is only a one by one matrix.

The pseudospectral matrices H_S and $H^\gamma_{\nu\kappa n}$ (for specific ν, κ, γ and n) are constructed from Eq. 1 with $\hat{H}$ replaced by $\hat{H}_S$ or $\hat{H}^\gamma_{\nu\kappa n}$, respectively (see appendix B for explicit forms of these

operators). These single elements are large matrices having dimensions set by the number of grid points. For multiple subdomains, they are block diagonal. The pseudospectral matrix is constructed for the subdomain's grid points. The number of columns and rows of an element equals the total number of grid points in all the subdomains.

The boundary conditions can be written as

$$\begin{pmatrix} B_0 & 0 \\ 0 & B_1 \end{pmatrix} \begin{pmatrix} g^0 \\ g^1 \end{pmatrix} = 0, \tag{C6}$$

where

$$B_\nu = \begin{pmatrix} B_\nu^{j_m} & 0 & \cdots & 0 \\ 0 & B_\nu^{j_{m+2}} & \ddots & \vdots \\ \vdots & \ddots & \ddots & 0 \\ 0 & \cdots & 0 & B_\nu^{j_M} \end{pmatrix}, \tag{C7}$$

is a diagonal matrix of the same size as H_ν^γ, and $j_m = \nu + \kappa_m + l + s$ and $j_M = \nu + \kappa_M + l + s$. Each B_ν^j is a rectangular matrix of the same width as $H_{\nu\kappa n}^\gamma$, but a smaller height corresponding to the number of grid points near internal boundaries or where a symmetry condition holds. If j is even (odd) B_ν^j enforces zero derivative (value) along the symmetry plane. Each of the B_ν^j matrices can be split into two sub-matrices and incorporated into the Hamiltonian matrix in the same way as in Ref. [1]

2. Matrix Eigenvalue Solution

The number of grid points in each sub-domain, $\{x, \phi, \theta_{12}\}$ or $\{x, \zeta, \beta_{12}\}$, was $n_t = 2n \times n \times n$; greater resolution is needed along the semi-infinite coordinate. This leads to a Hamiltonian matrix size of $n_t \times n_t$ for S states and $2n_t \times 2n_t$ for odd parity P states. After solving for boundary conditions, these are reduced to $n_m \times n_m$ and $2n_m \times 2n_m$, respectively, where $n_m = 6n^3 - 12n^2 + 6n$. The number of non-zero elements n_{NZ} scales as n^4. For $n = 20$, this corresponds to 560 MB and 1.8 GB, respectively, of memory required to store the matrix.[4] The largest matrix that was used to calculate an eigenvector was $86,640 \times 86,640$ and had $158,726,000$ non-zero elements.

[4] Note: some eigenvalue solvers do not require one to store this matrix and simply require a function which can calculate the matrix times a given vector.

The method of inverse iteration [22] was used to find eigenvalues with a shift equal to the known eigenvalues plus 10^{-4} so that the matrix is not too singular. Each iteration requires a matrix solve. For the smaller matrices (up to $17,000 \times 17,000$), these solves were performed using Mathematica's [32] multifrontal matrix solve routine. This method is fast (eigenvalues can be calculated in about 10 minutes for that size) but 8 GB of RAM was insufficient for larger sizes. For larger matrices, the *g*eneralized *m*inimal *res*idual (GMRES) method of PETSc [33–35] was used. The GMRES method produces a solution with the Krylov space of the matrix and is more memory efficient.

Preconditioning is essential for solving large matrix problems. A measure of how hard a matrix problem is to solve (how fast a method converges) is the spectral condition number, defined as

$$c = \frac{|\lambda_{\max}|}{|\lambda_{\min}|}, \tag{C8}$$

where $\lambda_{\max}$ and $\lambda_{\min}$ are the eigenvalues with the largest and smallest magnitudes, respectively. The spectral condition numbers of pseudospectral matrices grow rather fast with increasing resolution [36, 37]. For the problem at hand, it starts out large and grows asymptotically as n^{12} until it is about 10^{20} for $n = 23$. An ill-posed problem has a condition number which grows exponentially [38]. This problem is well-posed but in order to solve this system of equations preconditioning is necessary. A reasonable preconditioner is a matrix produced by a second order finite differencing scheme on the same set of grid points [21, 36, 37]. The preconditioning matrix solves are further preconditioned with a block Jacobi preconditioner.

The modified Gramm-Schmidt procedure was used to orthogonalize the Krylov subspace. Furthermore, the GMRES restart parameter, m, needs to be very large for convergence, empirically, $m = 1.3 n_m^{3/4}$, where $n_m \times n_m$ is the matrix size. The computation time scales as n_m^3, which for the largest matrix size was about a day running on six 2 GHz processors. The eigenvalue solver is the slowest part of the entire computation.

All calculations were done with double precision arithmetic. This gives some minimum error in the calculated eigenstate. The effect is relatively big for the small exponential tail. The key observation is that the wave function no longer decreases at the theoretically expected asymptotic rate when it drops to about $10^{-8.7}$ of its maximum value, after which it takes on a seemingly random value less than this magnitude. This value is independent of resolution because of the limits of machine precision arithmetic. It is possible that the asymptotic tail could be better calculated with a better preconditioner.

The issue of the asymptotic behavior is important. Since a constant value for the wave function on a semi-infinite domain leads to divergent matrix elements,[5] we set any value of the eigenvector below this threshold to zero.

3. Quadrature

In this article, it is necessary to calculate matrix elements of the form $\langle i|\hat{O}|j\rangle$, where $|i\rangle$ and $|j\rangle$ are two quantum states and $\hat{O}$ is some operator. This calculation requires numerical integration. Pseudospectral methods, by design, use quadrature points as the grid points. A one dimensional function $f[\mathrm{X}]$ can be numerically integrated from $\mathrm{X} = -1$ to $\mathrm{X} = 1$ with weight function $g[\mathrm{X}]$ by

$$\int_{-1}^{1} f[\mathrm{X}]g[\mathrm{X}]d\mathrm{X} \approx \sum w_i f[\mathrm{X}^i], \tag{C9}$$

where w_i is the quadrature weight specific to the weighting function g at grid point X^i. This quadrature formula is exponentially accurate with increasing resolution if f is smooth over the domain $-1 \leq \mathrm{X} \leq 1$. The problems solved in this article are three-dimensional with three overlapping subdomains. A separate quadrature can be done in each sub-domain. This is illustrated for domain D_1 with coordinates $\{x, \phi, \theta_{12}\}$ and ranges $-1 \leq x \leq 1$, $0 \leq \phi \leq 1/2$, and $0 \leq \theta_{12} \leq \pi$. Define

$$\mathrm{X}_1 = x \tag{C10}$$

$$\mathrm{X}_2 = 4\phi - 1 \tag{C11}$$

$$\mathrm{X}_3 = \frac{2\theta_{12}}{\pi} - 1, \tag{C12}$$

so that $-1 \leq \mathrm{X}_1, \mathrm{X}_2, \mathrm{X}_3 \leq 1$. Integrals over D_1 use three-dimensional sums analogous to Eq. C9. Since the ranges are fixed, the order of nesting is immaterial. To satisfy the requirement that f is smooth (up to the logarithmic singularity at $\rho = 0$), choose $g = 1$,[6] which corresponds to Legendre quadrature points, which are used for all calculations in this article instead of Chebyshev which were used in Ref. [1].

[5] For a finite resolution, the quadrature still leads to a finite result with an error enhanced by at most 10^4 for the cases calculated in this article.

[6] For each integral, one has an integrand, $\psi\hat{O}\psi$ times the factor from the volume element. This whole product is $f[X]g[X]$ so there is freedom as to how one divides the integrand between f and g up to the restriction that f be smooth. The simplest choice is made here.

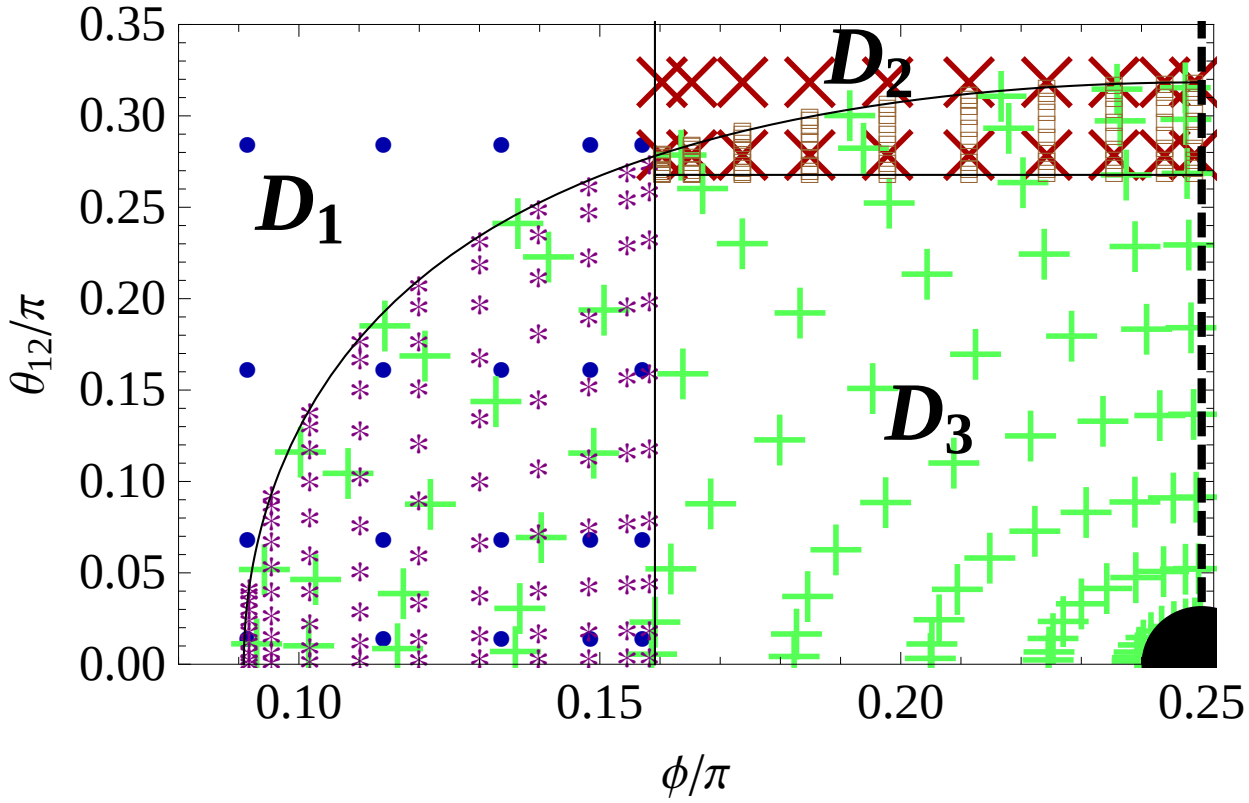

FIG. 5: (Color online). This is the arrangement of grid points of the three domains at a constant value of ρ in ϕ and θ_{12} coordinates for $n = 10$. As in Fig. 1, the blue circles, red crosses, and green pluses belong to domains D_1, D_2, and D_3, respectively. Also shown are the overlap grid points in $D_1 \cap D_3$ (purple stars) and $D_2 \cap D_3$ (brown squares). The electron-electron singularity is visible at the lower right hand corner (solid disk at $\phi = \pi/4, \theta_{12} = 0$) as well as the line of symmetry on the right side (dashed line at $\phi = \pi/4$ where $r_1 = r_2$).

If all the subdomains are non-overlapping, then the above scheme is sufficient for all integrals. However, no set of non-overlapping subdomains for which f is smooth could be found.[7] A method is needed for handling overlapping regions, which the above scheme double counts if a quadrature is performed in each sub-domain. For these regions, an interpolation was performed to two new $2n \times n \times n$ grids spanning the overlap regions, shown in Fig 5. For the pseudospectral method, interpolation is done to the same order as the grid size. A quadrature can then be done over the overlap regions, which are used to correct the overall

[7] Some do exist which are only non-analytic on some edges, but these produce noticeable non-exponential convergence.

integration.

The overlap region is divided into two subdomains

$$D_{13} \;=\; D_1 \cap D_3 \tag{C13}$$

$$D_{23} \;=\; D_2 \cap D_3. \tag{C14}$$

These subdomains satisfy

$$\begin{aligned} D_{13}:\; & -1 \le x \le 1,\; \phi_{\min} \le \phi \le \tfrac{1}{2}, \qquad 0 \le \theta_{12} \le \theta_{12,\max}[\phi] \\ D_{23}:\; & -1 \le x \le 1, \quad \tfrac{1}{2} \le \phi \le \tfrac{\pi}{4}, \quad \arccos\tfrac{2}{3} \le \theta_{12} \le \theta_{12,\max}[\phi], \end{aligned} \tag{C15}$$

where $\phi_{\min} = \pi/4 - 1/2$ is determined by $\zeta = 1/2$ and $\theta_{12} = 0$ and $\theta_{12,\max}[\phi] = \arccos[\cos 1 \csc 2\phi]$ is determined by $\zeta = 1/2$. One defines appropriate $\{\mathrm{X}_1, \mathrm{X}_2, \mathrm{X}_3\}$. For example, in D_{13}

$$\mathrm{X}_1 \;=\; x \tag{C16}$$

$$\mathrm{X}_2 \;=\; 2\left(\frac{\phi - \phi_{\min}}{\frac{1}{2} - \phi_{\min}}\right) - 1 \tag{C17}$$

$$\mathrm{X}_3 \;=\; 2\theta_{12,\max}[\phi]\theta_{12} - 1. \tag{C18}$$

Now one calculates the nested sum with X_3 innermost since the range of θ_{12} depends upon ϕ.

The function values at the points necessary for the quadrature $\{x^{j_1'}, \phi^{j_2'}, \theta_{12}^{j_2' j_3'}\}$ are calculated with interpolation

$$f[x^{j_1'}, \phi^{j_2'}, \theta_{12}^{j_2' j_3'}] \approx \sum_J f[x^{j_1}, \phi^{j_2}, \theta_{12}^{j_3}] \mathcal{C}_J[x^{j_1'}, \phi^{j_2'}, \theta_{12}^{j_2' j_3'}]. \tag{C19}$$

where $\mathcal{C}_J$ refers to the effective basis defined in Eq. A3 and $J = \{j_1, j_2, j_3\}$.

Sometimes f involves a Dirac delta function. In such a case, one integrates out the delta function analytically. One is left with a two dimensional integral on the surface where the argument of the delta function is zero. This entails first interpolating to that surface using Eq. C19. One can then proceed normally with a two-dimensional quadrature.

Appendix D: Calculating matrix elements with Bhatia and Temkin's radial functions

1. Oscillator Strength

In the Bhatia and Temkin three-three splitting [24], the matrix elements for an $^1\mathrm{S} \rightarrow {}^1\mathrm{P}$ oscillator strength transition are written:

$$\sum_m |\langle {}^1\mathrm{S}|\hat{\mathbf{D}}|{}^1\mathrm{P}m\rangle|^2 = \left[\int d\tau g^0_{000}\left(d^0_D g^0_{110} + d^1_D g^1_{110}\right)\right]^2, \tag{D1}$$

where $d\tau = r_1^2 r_2^2 \sin\theta_{12} dr_1 dr_2 d\theta_{12}$, $\hat{\mathbf{D}}$ is one of the operators found inside the matrix elements of Eqs. 7 and the operators d^i_D are given by

$$d^0_{\mathbf{R}} = (r_1 + r_2)\cos\frac{\theta_{12}}{2} \tag{D2}$$

$$d^1_{\mathbf{R}} = (r_1 - r_2)\sin\frac{\theta_{12}}{2} \tag{D3}$$

$$\begin{aligned} d^0_{\mathbf{P}} = {} & \frac{(r_1 + r_2)(3 + \cos\theta_{12})}{4 r_1 r_2 \cos\frac{\theta_{12}}{2}} \\ & + \cos\frac{\theta_{12}}{2}\left(\frac{\partial}{\partial r_1} + \frac{\partial}{\partial r_2}\right) \\ & - \frac{(r_1 + r_2)\sin\frac{\theta_{12}}{2}}{r_1 r_2}\frac{\partial}{\partial\theta_{12}} \end{aligned} \tag{D4}$$

$$\begin{aligned} d^1_{\mathbf{P}} = {} & \frac{(r_1 - r_2)(-3 + \cos\theta_{12})}{4 r_1 r_2 \sin\frac{\theta_{12}}{2}} \\ & + \sin\frac{\theta_{12}}{2}\left(\frac{\partial}{\partial r_1} - \frac{\partial}{\partial r_2}\right) \\ & - \frac{(r_1 - r_2)\cos\frac{\theta_{12}}{2}}{r_1 r_2}\frac{\partial}{\partial\theta_{12}} \end{aligned} \tag{D5}$$

$$d^0_{\mathbf{A}} = \frac{Z(r_1^2 + r_2^2)\cos\frac{\theta_{12}}{2}}{r_1^2 r_2^2} \tag{D6}$$

$$d^1_{\mathbf{A}} = \frac{Z(r_1^2 - r_2^2)\sin\frac{\theta_{12}}{2}}{r_1^2 r_2^2}. \tag{D7}$$

2. Expectation Values

Similarly, an expectation value for an S state is calculated by

$$\langle {}^1\mathrm{S}|\hat{\mathbf{D}}|{}^1\mathrm{S}\rangle = \int d\tau g^0_{000} d^0_D g^0_{000}. \tag{D8}$$

Most of the operators d_D^0 used for expectation values in this article have trivial forms. We write here only the two most complicated ones:

$$\begin{aligned} d^0_{\mathbf{p}_1\cdot\mathbf{p}_2} &= \frac{1}{r_1 r_2}\left[\sin\theta_{12}\left(r_1\frac{\partial}{\partial r_1}+r_2\frac{\partial}{\partial r_2}\right)\frac{\partial}{\partial\theta_{12}}\right. \\ &\quad -r_1 r_2\cos\theta_{12}\frac{\partial^2}{\partial r_1\partial r_2}+\cos\theta_{12}\frac{\partial^2}{\partial {\theta_{12}}^2} \\ &\quad \left.+\frac{1}{\sin\theta_{12}}\frac{\partial}{\partial\theta_{12}}\right] \qquad \text{(D9)} \\ d^0_{H_{OO}} &= -\frac{\alpha^2}{2r_{12}^3}\left[\sin\theta_{12}\left(x_{12}\frac{\partial}{\partial r_1}+x_{21}\frac{\partial}{\partial r_2}\right)\frac{\partial}{\partial\theta_{12}}\right. \\ &\quad +r_1 r_2 z_+\frac{\partial^2}{\partial r_1\partial r_2}+z_-\frac{\partial^2}{\partial {\theta_{12}}^2} \\ &\quad \left.+\frac{r_{12}^2}{r_1 r_2\sin\theta_{12}}\frac{\partial}{\partial\theta_{12}}\right], \qquad \text{(D10)} \end{aligned}$$

where

$$x_{ij}=\frac{r_i^2+r_{12}^2-\mathbf{r}_1\cdot\mathbf{r}_2}{r_j} \qquad \text{(D11)}$$

and

$$z_\pm=(1\pm 3)\cos\theta_{12}(\cos\theta_{12}-\rho^2/2r_1r_2)+\sin^2\theta_{12}. \qquad \text{(D12)}$$

All of these forms must be converted to the appropriate coordinates in each subdomain.

Acknowledgments

We thank Harald P. Pfeiffer for help in solving large pseudospectral matrix problems, Saul Teukolsky and Cyrus Umrigar for guidance and support, and Charles Schwartz for useful comments on the manuscript. This material is based upon work supported by the National Science Foundation under Grant No. AST-0406635 and by NASA under Grant No. NNG-05GF79G.

[1] P. E. Grabowski and D. F. Chernoff, Phys. Rev. A, **81**, 032508 (2010).

[2] J. H. Bartlett, Phys. Rev., **51**, 661 (1937).

[3] V. A. Fock, Izv. Akad. Nauk. SSSR, Ser. Fiz, **18**, 161 (1954).

[4] V. A. Fock, K. Nor. Vidensk. Selsk. Forh, **31**, 145 (1958).

[5] C. Canuto, M. Hussaini, A. Quarteroni, and T. Zang, Spectral Methods in Fluid Dynamics (Springer, Berlin, 1988).

[6] L. E. Kidder and L. S. Finn, Phys Rev. D, **62**, 084026 (2000).

[7] H. P. Pfeiffer, L. E. Kidder, M. A. Scheel, and S. A. Teukolsky, Comput. Phys. Commun., **152**, 253 (2003), ISSN 0010-4655.

[8] R. A. Friesner, Chem. Phys. Lett., **116**, 39 (1985), ISSN 0009-2614.

[9] R. A. Friesner, J. Chem. Phys., **85**, 1462 (1986).

[10] R. A. Friesner, J. Chem. Phys., **86**, 3522 (1987).

[11] M. N. Ringnalda, M. Belhadj, and R. A. Friesner, J. Chem. Phys., **93**, 3397 (1990).

[12] B. H. Greeley, T. V. Russo, D. T. Mainz, R. A. Friesner, J.-M. Langlois, W. A. Goddard, III, J. Robert E. Donnelly, and M. N. Ringnalda, J. Chem. Phys., **101**, 4028 (1994).

[13] R. B. Murphy, M. D. Beachy, R. A. Friesner, and M. N. Ringnalda, J. Chem. Phys., **103**, 1481 (1995).

[14] R. B. Murphy, Y. Cao, M. D. Beachy, M. N. Ringnalda, and R. A. Friesner, J. Chem. Phys., **112**, 10131 (2000).

[15] C. Ko, D. K. Malick, D. A. Braden, R. A. Friesner, and T. J. Martínez, J. Chem. Phys., **128**, 104103 (2008).

[16] J. S. Heyl and A. Thirumalai, Mon. Not. R. Astron. Soc. (2010).

[17] A. G. Borisov, J. Chem. Phys., **114**, 7770 (2001).

[18] J. P. Boyd, C. Rangan, and P. H. Bucksbaum, J. Comput. Phys., **188**, 56 (2003), ISSN 0021-9991.

[19] J. P. Boyd, Chebyshev and Fourier Spectral Methods, 2nd ed. (Dover, Mineola, New York 11501, 2000).

[20] B. Fornberg, A Practical Guide to Pseudospectral Methods (Cambridge University Press, 40 West 20th Street, New York, NY 10011-4211, 1996).

[21] S. A. Orszag, Journal of Computational Physics, **37**, 70 (1980).

[22] W. H. Press, S. A. Teukolsky, W. T. Vetterling, and B. P. Flannery, Numerical Recipes: The Art of Scientific Computing, 3rd ed. (Cambridge University Press, 32 Avenue of the Americas, New York, NY 10013-2473, USA, 2007).

[23] V. E. A. Hylleraas, Z. Phys., **54**, 347 (1929).

[24] A. K. Bhatia and A. Temkin, Rev. Mod. Phys., **36**, 1050 (1964).

[25] A. Hibbert, Rep. Prog. Phys., **38**, 1217 (1975).

[26] B. Schiff, C. L. Pekeris, and Y. Accad, Phys. Rev. A, **4**, 885 (1971).

[27] E. A. Coddington, "An introduction to ordinary differential equations," (General Publishing Company, Ltd., Toronto, Ontario, 1961) Chap. 4.

[28] C. R. Myers, C. J. Umrigar, J. P. Sethna, and J. D. Morgan, Phys. Rev. A, **44**, 5537 (1991).

[29] C. Schwartz, Int. J. of Mod. Phys. E, **15**, 877 (2006).

[30] G. W. F. Drake, in Atomic, Molecular, and Optical Physics Handbook, edited by G. W. F. Drake (American Institute of Physics, 1996).

[31] M. Žitnik, A. Stanič, K. Bučar, J. G. Lambourne, F. Penent, R. I. Hall, and P. Lablanquie, Journal of Physics B: Atomic, Molecular and Optical Physics, **36**, 4175 (2003).

[32] I. Wolfram Research, Mathematica, version 7.0 (Wolfram Research, Inc., Champaign, Illinois, 2008).

[33] S. Balay, K. Buschelman, W. D. Gropp, D. Kaushik, M. G. Knepley, L. C. McInnes, B. F. Smith, and H. Zhang, "PETSc Web page," (2009), http://www.mcs.anl.gov/petsc.

[34] S. Balay, K. Buschelman, V. Eijkhout, W. D. Gropp, D. Kaushik, M. G. Knepley, L. C. McInnes, B. F. Smith, and H. Zhang, PETSc Users Manual, Tech. Rep. ANL-95/11 - Revision 3.0.0 (Argonne National Laboratory, 2008).

[35] S. Balay, W. D. Gropp, L. C. McInnes, and B. F. Smith, in Modern Software Tools in Scientific Computing, edited by E. Arge, A. M. Bruaset, and H. P. Langtangen (Birkhäuser Press, 1997) pp. 163–202.

[36] H. P. Pfeiffer, "personal communication," (2010).

[37] B. Fornberg, "A practical guide to pseudospectral methods," (Cambridge University Press, 40 West 20th Street, New York, NY 10011-4211, 1996) Chap. 5.4.

[38] S. A. Teukolsky, "personal communication," (2010).